jmp STATISTICAL DISCOVERY

The Relevance of Measurement Systems Analysis

A Procter & Gamble Case Study on MSA Methodology and Applications

DATE
OCTOBER 10 AND 12

TIME
16:00 CET, 10 am EST

CHRISTIAN NEU
Scientist
Procter & Gamble

JERRY FISH
Systems Engineer
JMP

JASON WIGGINS
Senior Systems Engineer
JMP

Register now

Chemical Engineering & Technology Research Article 1

Jörg Kressler[1,*]
Julian Radicke[1]
Karsten Busse[1]
Konstantin Amsharov[1]
Yury Golitsyn[1]
Detlef Reichert[1]
Frank Syrowatka[2]
Nazmul Hasan[1]

Synthesis and Characterization of ^{15}N-Labeled Poly(sulfur nitride) in Bulk and in Superconductor Composites

^{15}N-labeled tetrasulfur tetranitride ($S_4{}^{15}N_4$) was synthesized by reacting S_2Cl_2 with $^{15}NH_3$. The reaction was finalized with $^{14}NH_3$. The successful labeling was confirmed by solution ^{15}N nuclear magnetic resonance (NMR) spectroscopy. $S_4{}^{15}N_4$ was used for the synthesis of poly(sulfur nitride) $S^{15}N_x$ via the intermediate species of S_2N_2. It was a topochemical polymerization in the solid state. The isotope ratio in the labeled polymer was obtained by laser deposition ionization time-of-flight mass spectroscopy. Solid-state ^{15}N NMR spectroscopy of $S^{15}N_x$ indicates that at least three different chemical environments for ^{15}N atoms are present in the crystals. Finally, SN_x was polymerized in the presence of two other superconductors, MgB_2 and yttrium barium copper oxide (YBCO), which demonstrates the capability of SN_x for grain boundary engineering.

Keywords: Laser deposition ionization time-of-flight, ^{15}N solid-state NMR, Poly(sulfur nitride), Solid-state polymerization

Received: March 08, 2023; *revised:* June 01, 2023; *accepted:* June 29, 2023

DOI: 10.1002/ceat.202300141

1 Introduction

Due to the high electrical conductivity at room temperature in the range of $10^3\,S\,cm^{-1}$, which is only two orders of magnitude less than that of copper [1], and the superconductivity below 0.23 K [2], poly(sulfur nitride) (SN_x) was extensively studied from an experimental and theoretical point of view [3, 4]. In contrast to other conductive polymers that are usually insulators in their native state [5], SN_x does not need any reduction or oxidation steps (doping) to achieve the high electrical conductivity at room temperature. Over the years, several reviews on SN_x have been published [6–9]. Nevertheless, our knowledge on the chemical structure of SN_x in the solid state is very limited. Small-angle X-ray scattering (SAXS) and small-angle neutron scattering (SANS) data provide the crystal structure [10, 11]. Extensive micro- and macro-twinning complicates the situation extremely as single crystals are limited to nanometer dimensions [12]. Some electrical, magnetic, and optical properties have been studied in detail [5]. In contrast, nothing has been known about chain defects, molar masses, and end groups of SN_x. The main reasons are: (i) SN_x is not soluble in any solvent, and (ii) the available nuclei that are suitable for solid-state nuclear magnetic resonance (NMR) spectroscopy have a very small natural abundance. So, an adequate way for further polymer characterization is the polymer labeling with ^{15}N. This can relatively easily be achieved by using $^{15}NH_3$ for the synthesis of tetrasulfur tetranitride (S_4N_4), which is then converted to disulfur dinitride (S_2N_2) using Ag_2S as a catalyst at elevated temperatures. S_2N_2 is then the monomer for spontaneous topochemical solid-state polymerization of SN_x [5].

Here, we deal with the synthesis and characterization of ^{15}N-labeled $S_4{}^{15}N_4$ and $S^{15}N_x$. $S_4{}^{15}N_4$ is characterized by infrared (IR) and Raman spectroscopy and both $S_4{}^{15}N_4$ and $S^{15}N_x$ are analyzed by solid-state ^{15}N NMR spectroscopy. Finally, SN_x is prepared and characterized in the presence of two superconductors, yttrium barium copper oxide (YBCO) [13] and MgB_2 [14], respectively.

2 Experimental

2.1 Materials

The synthesis of $S_4{}^{14}N_4$ is described in detail elsewhere [15]. $S_4{}^{15}N_4$ was synthesized in a three-neck flask with 400 mL dry chloroform. Then 40 mL S_2Cl_2 was added. The flask was equipped with a stirrer, a gas inlet pipe, and a reflux condenser. Prior to the reaction, the flask was flashed for 10 min with nitrogen. The $^{15}NH_3$ gas (Eurisotop, Saint-Aubin, France;

[1]Prof. Dr. rer. nat. habil. Jörg Kressler (joerg.kressler@chemie.uni-halle.de), Julian Radicke, Dr. rer. nat. Karsten Busse, Prof. Dr. Konstantin Amsharov, Dr. Yury Golitsyn, Prof. Dr. Detlef Reichert, Dr. Nazmul Hasan
Faculty of Natural Science II, Chemistry, Physics, and Mathematics, Martin Luther University Halle-Wittenberg, 06099 Halle (Saale), Germany.

[2]Frank Syrowatka
Interdisciplinary Center of Materials Science, Martin Luther University Halle-Wittenberg, 06099 Halle (Saale), Germany.

99.4 % ^{15}N) was bubbled into the solution and the flask was cooled with an ice bath in order to keep the reaction solution at room temperature. The ^{15}N-labeled ammonia that was not consumed during the bubbling was collected in a rubber ball and reused several times. After 2.5 h, the reaction solution changed to orange color. Then, for another 4 h, non-labeled ammonia was added in order to complete the reaction. The solution was then poured into distilled water and filtered for the removal of NH_4Cl, and 18.59 g of the filtrate, which is a mixture of sulfur and S_4N_4, was purged with N_2 and dried at room temperature. The further cleaning and characterization of $S_4{}^{15}N_4$ is discussed below. The two superconductors, YBCO ($YBa_2Cu_3O_x$, x ~6.7–9.5) and magnesium diboride (MgB_2), were purchased from Sigma-Aldrich. Tablets were prepared in a hydraulic press at room temperature. During the preparation of the composite superconductors, the stream of S_2N_2 was directed over the superconductor tablets.

2.2 Analytical Methods

2.2.1 Conductive Atomic Force Microscopy

A MultiMode 8 instrument from Bruker (Santa Barbara, USA) coupled with a PeakForce tunneling (PF-TUNA) module was used to perform conductive atomic force microscopy (AFM) measurements. SN_x deposited on the YBCO substrate has two sides, and the side with a more golden hue was initially identified using optical microscopy. This side was kept upward, while the other side of the substrate was attached to a metal disc with double-sided adhesive tape. Colloidal silver paint was used to contact the substrate to the metal disc. An SCM-PIT-V2 conductive probe with a spring constant of 3 N m^{-1} and a resonant frequency of 75 kHz was used. The direct current (DC) bias voltage applied was 800 mV. All of the AFM measurements were carried out at 1 kHz oscillation in air. Images were taken with lateral resolutions of 512 pixels at a scanning rate of 0.5 Hz. The software program Gwyddion [16] was used to process the AFM images. Two different images were presented such as the height image, which provides the surface topography along with height information, and the TUNA current map, which provides the average local conductivity of the sample.

2.2.2 Confocal Raman Microscopy

Confocal Raman microscopy was performed with a Renishaw in-Via Raman microscope (Renishaw plc, UK). A Leica DMI 3000 inverted microscope (Leica Microsystems GmbH, Germany) was equipped with a charge-coupled device (CCD) camera. The Cobolt CW DPSS laser had a wavelength of 532 nm and a grating of 1800 L mm^{-1}. Before starting the experiments, the Raman spectrometer was calibrated to a silicon reference peak and the signal was adjusted to 520.4 cm^{-1}. Every spectrum was recorded between 150 and 1200 cm^{-1} with 1.0 % laser intensity and 10 s of integration time for all SN_x and S_4N_4 samples (with and without ^{15}N).

2.2.3 Fourier Transform Infrared Spectroscopy

A Bruker Vector 22 (Bruker Optik GmbH, Germany) spectrometer was used to perform Fourier transform infrared (FTIR) experiments for both the S_4N_4 and $S_4{}^{15}N_4$ samples. The experiments were carried out in transmission mode in KBr at room temperature. The spectra were recorded in the wavenumber range of 4000–400 cm^{-1} with 256 scans at a resolution of 4 cm^{-1}.

2.2.4 Solution ^{15}N NMR Spectroscopy

The solution ^{15}N NMR measurement of $S_4{}^{15}N_4$ in $CDCl_3$ was performed on an Agilent Technologies 500 MHz DD2 spectrometer at 27 °C. Calibration to liquid NH_3 was performed and 380.5 ppm was subtracted to set the values to a CH_3NO_2 standard. Evaluation and display of the spectrum were carried out via MestReNova 9.0.1.

2.2.5 Solid-State ^{15}N NMR Spectroscopy

Solid-state ^{15}N NMR static experiments were performed on a Bruker Avance 400 spectrometer, operating at a ^{15}N Larmor frequency of 40.56 MHz. The temperature was controlled by a BVT-3000 heating device with an accuracy of ±1 °C. For all experiments the temperature was set to 25 °C. A static double-resonance probehead with a 5-mm coil was used. For the polymer sample SN_X, the ^{15}N $\pi/2$ pulse length was 9 µs and the recycle delay was 60 s. 8192 scans were accumulated. For the monomer S_4N_4 sample, a ^{15}N $\pi/2$ pulse of 9 µs length and a recycle delay of 30 min were applied. No signal could be detected for shorter repetition times. 1024 scans were accumulated. For both samples, the Hahn echo delay was 100 µs. The spectrum was referenced according to the NH resonance of ^{15}N-labeled butoxycarbonyl (BOC)-glycine (R_{iso} = 75.5 ppm).

2.2.6 Laser Deposition Ionization Time-of-Flight Mass Spectroscopy

Laser deposition ionization time-of-flight (LDI-ToF) mass spectra were recorded directly from the solid-state samples without using a matrix on the Axima Confidence spectrometer (Shimadzu, Japan).

2.2.7 X-Ray Measurements

A crystal with approximate dimensions of 0.30 mm × 0.30 mm × 0.50 mm was mounted on a glass fiber. The intensity data were taken from this sample using a STOE-IPDS diffractometer with Mo-Kα radiation (λ = 0.7103 Å, graphite monochromator) at T = 170 K, and 120 individual scans were performed during sample rotation to obtain a 3D scattering pattern.

2.2.8 Scanning Electron Microscopy, Energy Dispersive X-Ray Analysis, and Polarized Optical Microscopy

Scanning electron microscopy (SEM) was carried out with a GEMINI SEM 500 from Carl-Zeiss Microscopy GmbH. The imaging was carried out with an acceleration voltage of 3 kV. Backscattered electrons were used for the material contrast and secondary electrons for the topography contrast during imaging. The scanning electron microscope was equipped with an energy dispersive X-ray (EDX) analysis system from Oxford. The detector was the windowless extreme detector at 3 kV excitation energy and a very short measurement time of 1 s per spectrum in order to minimize radiation damage of the polymer. Polarized optical microscopy (POM) was carried out using a SteREO Discovery microscope (Carl Zeiss, Jena, Germany) equipped with a polarization filter and analyzer.

3 Results and Discussion

Starting point for the synthesis of SN_x is the preparation of S_4N_4 (Fig. 1a) by reacting S_2Cl_2 with ammonia (NH_3) in chloroform [15]. Since the natural abundance of nitrogen isotopes is 99.6 % ^{14}N and 0.4 % ^{15}N, the non-labeled species is called $^{14}NH_3$. The ^{15}N-labeled species is called $^{15}NH_3$. It should be noted that sulfur has four stable isotopes, where the most frequent isotopes are ^{32}S with 95.02 % and ^{34}S with 4.21 %.

$$6\ S_2Cl_2 + 16\ ^{14}NH_3 \rightarrow S_4^{14}N_4 + S_8 + 12\ ^{14}NH_4Cl \quad (1)$$

$$6\ S_2Cl_2 + 16\ ^{15}NH_3 \rightarrow S_4^{15}N_4 + S_8 + 12\ ^{15}NH_4Cl \quad (2)$$

S_4N_4 adopts a 'cradle' structure, i.e., a strongly deformed eight-membered ring of alternating sulfur and nitrogen atoms, where the S–S pairs have weak transannular interactions. For purification of S_4N_4, the reaction products were washed with distilled water in order to remove NH_4Cl [15]. The remaining precipitate in chloroform was filtered, dissolved in hot toluene and slowly cooled to room temperature. This leads to the separate formation of large sulfur and S_4N_4 crystals (Fig. 1b), which can be collected separately. Similar to sulfur, S_4N_4 has a thermochromic effect [17], i.e., the crystals are orange at room temperature (Fig. 1c) and they become yellow (Fig. 1d) when cooled with liquid N_2. The successful labeling of $S_4{}^{15}N_4$ is confirmed by ^{15}N NMR solution spectroscopy (Fig. 1e). The occurrence of a single peak at 124.8 ppm is in agreement with literature data [18]. Furthermore, an $S_4{}^{15}N_4$ single crystal (Fig. 1f) is measured at 170 K by X-ray diffraction and yields a monoclinic unit cell with the space group $P2_1/n$ in agreement with reference [19]. Wide-angle X-ray scattering (WAXS) measurements on a nearly perfect single crystal of $S_4{}^{15}N_4$ show a proper reciprocal crystal structure (projection in c^*-direction in Fig. 1g). The unit cell was identified as monoclinic with $a = 8.65$ Å, $b = 7.11$ Å, $c = 8.7$ Å, and $\beta = 93.2°$, in good agreement with the cell parameters published by Scherer et al. [17] for $S_4{}^{14}N_4$. There is still some amount of background signal, showing some small defects of the crystal. The quality of the obtained pattern is not sufficient to obtain reliable atom positions within the unit cell. In summary, the structural properties of $S_4{}^{14}N_4$ and $S_4{}^{15}N_4$ are completely identical.

For further purification, all S_4N_4 samples were sublimated at 30 °C and 2–3 mbar (see inset of Fig. 2a). The purity of $S_4{}^{14}N_4$ and $S_4{}^{15}N_4$ can be verified by FTIR and Raman spectroscopy. The occurrence of all bands below 1000 cm^{-1} is characteristic

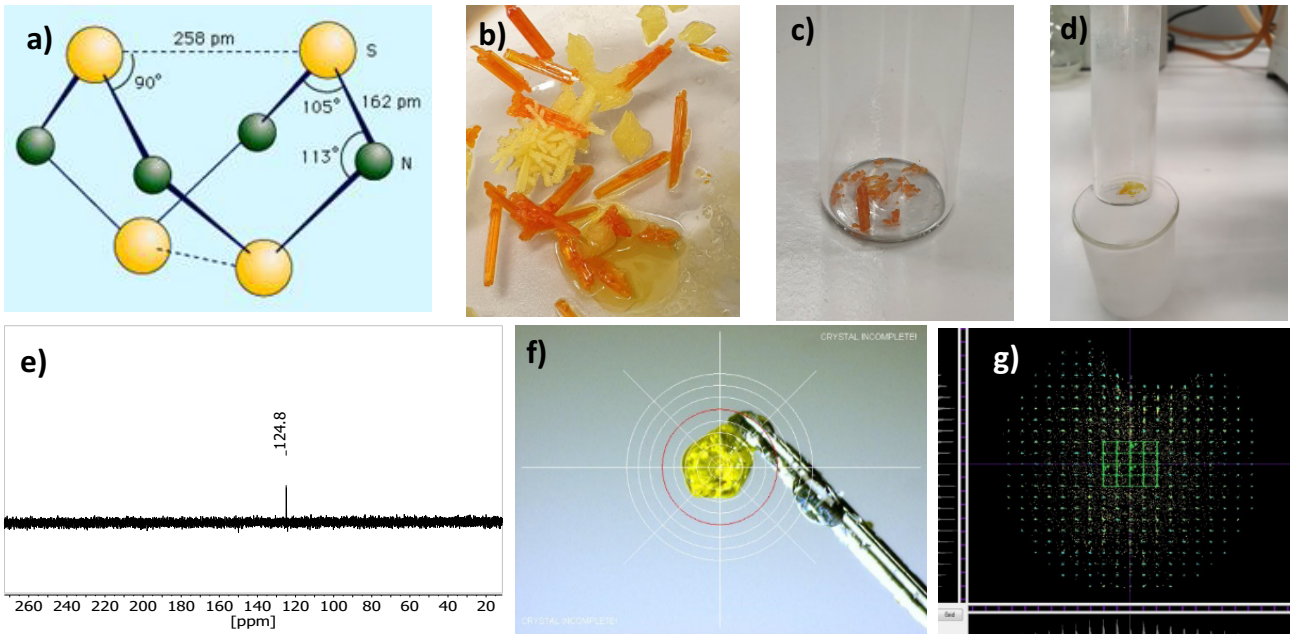

Figure 1. a) Chemical structure of S_4N_4 (Encyclopedia Britannica), b) photograph of sulfur and S_4N_4 crystals prepared by slow cooling from hot toluene solution to room temperature. c) $S_4{}^{15}N_4$ crystals at room temperature, d) $S_4{}^{15}N_4$ crystals cooled with liquid nitrogen, e) ^{15}N NMR spectrum of $S_4{}^{15}N_4$ obtained in $CDCl_3$ at room temperature, f) $S_4{}^{15}N_4$ single crystal at 170 K, g) c^*-projection of the 3D X-ray scattering pattern of the crystal shown in (f).

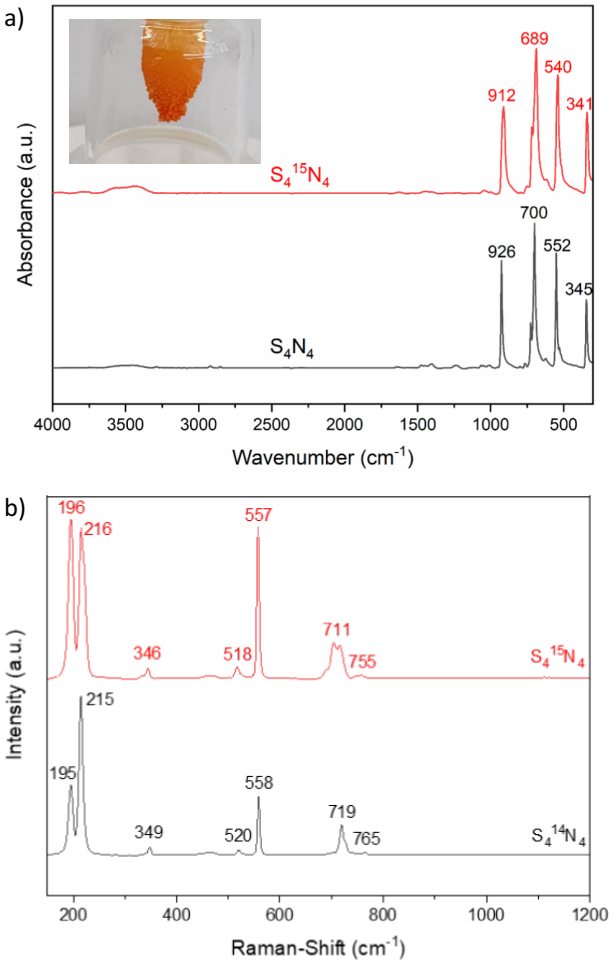

Figure 2. a) FTIR spectra of $S_4{}^{14}N_4$ and $S_4{}^{15}N_4$ and b) the respective Raman spectra. The inset in (a) shows $S_4{}^{15}N_4$ crystals grown on a cooling finger after sublimation.

of the FTIR spectra (Fig. 2a). The appearance of bands above 1000 cm^{-1} would indicate impurifications as, e.g., oxidation products. Raman spectra show signals below 800 cm^{-1} (Fig. 2b). All systematic shifts of the bands in the FTIR and Raman spectra between $S_4{}^{14}N_4$ and $S_4{}^{15}N_4$ are caused by the different masses of the ^{14}N and ^{15}N isotopes [20].

In the next step, S_4N_4 is sublimated in vacuum at elevated temperatures over silver wool and initially forms Ag_2S, which acts as catalyst for the transformation of S_4N_4 to S_2N_2 (Fig. 3a) in the gas phase [5]. Due to the explosive character of S_4N_4 and S_2N_2, the amount used in further experiments is limited to 1 g [21]. Then, the monomer S_2N_2 crystallizes in a cooling trap filled with liquid nitrogen and the topochemical ring opening polymerization to SN_x occurs for 3 days. To finalize the polymerization, the crystals are kept in the dark at room temperature over several weeks [5]. The crystals appear on the glass surface of the cooling finger and eventually fall down to the bottom (Fig. 3b). During the course of polymerization, they change color from white to black to golden metallic. Typical crystals observed by POM are shown in Fig. 3c,d. The crystals have a metallic gloss along the polymer chain directions and appear blue/black perpendicular to the chain direction, as can be observed in the twin crystal of Fig. 3d. Both, the S_2N_2 monomer and the SN_x polymer crystallize in a monoclinic unit cell with the $P2_1/c$ space group [8]. Upon polymerization, the unit cell volume decreases by 7 %. Due to the anisotropic cell shrinkage, microfibrillar crystallites are formed [10]. SN_x shows an extensive twinning behavior, which complicates the crystallographic analysis and its relation to other physical polymer properties [12].

SN_x is a polymer with properties of a semi-metal. The electrical DC conductivity at room temperature is in the range of 10^3 S cm^{-1}, which is only two orders of magnitude less than that of copper. It is generally accepted that SN_x is not soluble in any solvent. Thus, the polymer characterization is limited to solid-state techniques. A good method to check the quality of the synthesized SN_x crystals is Raman spectroscopy (Fig. 4).

The Raman spectra are in agreement with literature data [22]. Similar to the S_4N_4 case, the labeling with ^{15}N leads to a systematic shift of the Raman spectra when comparing $S^{14}N_x$ and $S^{15}N_x$. It should be noted that we were not able to obtain proper FTIR spectra of SN_x. Due to the metallic character there are problems to obtain IR spectra in typical reflectance modes. As discussed by Macklin et al. [20], SN_x degrades when imbedded in KBr for typical transmission mode measurements.

As discussed in the experimental part, the synthetic procedure for labeled $S_4{}^{15}N_4$ was started with $^{15}NH_3$ and finalized with $^{14}NH_3$. Thus, the ratio of ^{14}N to ^{15}N in the labeled $S^{15}N_x$ remains an open question, which can be answered by LDI-ToF experiments.

LDI-ToF mass spectra obtained from $S^{15}N_x$ and $S^{14}N_x$ are shown in Fig. 5. Since SN_x is not soluble in any matrix, the measurements were carried out without imbedding the polymer. The background-corrected mass spectrum shows only fragments of the type S_xN_y with $y = x$ or $y = x \pm 1$, indicating that all fragments come from an alternating SN structure. The observed fragments range from S_2N to S_8N_8. Within each S_xN_y

Figure 3. a) Chemical structure of S_2N_2, b) formation of SN_x crystals in the cooling trap, c) POM of an SN_x crystal, d) POM image of an SN_x twin crystal.

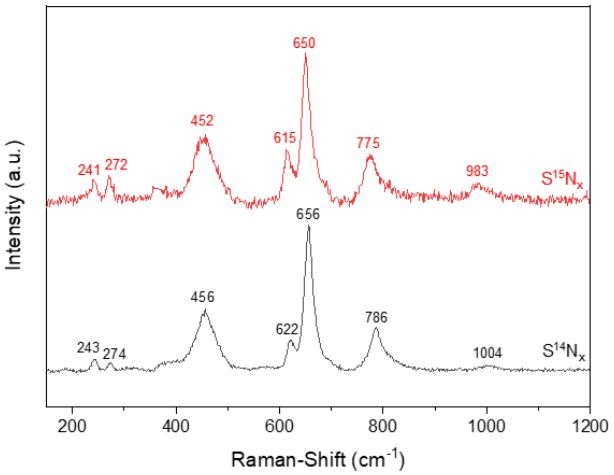

Figure 4. Raman spectra of $S^{14}N_x$ and $S^{15}N_x$.

fragment, a mass splitting according to the natural abundance of N and S isotopes for $S^{14}N_x$ was observed, most prominently indicated by the appearance of a second peak for the small amount of natural ^{34}S. For the labeled $S^{15}N_x$, the enrichment of ^{15}N isotopes was determined by the splitting of the S_2N signal to 57.5 % ^{15}N and 42.5 % ^{14}N (inset). The splitting of the other fragments is in good agreement with the obtained nitrogen isotope ratio, including the natural abundance of sulfur isotopes.

It has been known from the literature that sulfur-nitrogen compounds can explode during the measurement and thus damage the measuring equipment [23]. Therefore, ^{15}N magic-angle spinning (MAS) NMR spectra could not be recorded. Furthermore, the sulfur-nitrogen compounds do not contain hydrogen atoms, which make magnetization transfer from protons to the ^{15}N nuclei impossible. This results only in experiments with direct excitation and long waiting times between scans being available for sample characterization. Due to large chemical shift anisotropy (CSA) in static experiments, the ^{15}N spectra exhibit very broad lines (hundreds of ppm). Combined with the long dead time of the probehead, this leads to distortion of the baseline after the Fourier transformation. To avoid this problem, the Hahn echo experiment was used to record the spectra. The echo delay was adjusted to observe the full echo signal and then Fourier transformed from the echo maximum. As a result, a straight baseline without distortions was obtained. Fig. 6a shows the static ^{15}N NMR spectrum of $S_4{}^{15}N_4$, which exhibits the typical powder pattern with positive shielding anisotropy. The fit using *Dmfit* software [24] provides the following values: isotropic chemical shift R_{iso} = 123.9 ppm, anisotropy $\Delta CSA = R_{zz} - R_{iso}$ = –94.2 ppm, and the asymmetry η = 0.44.

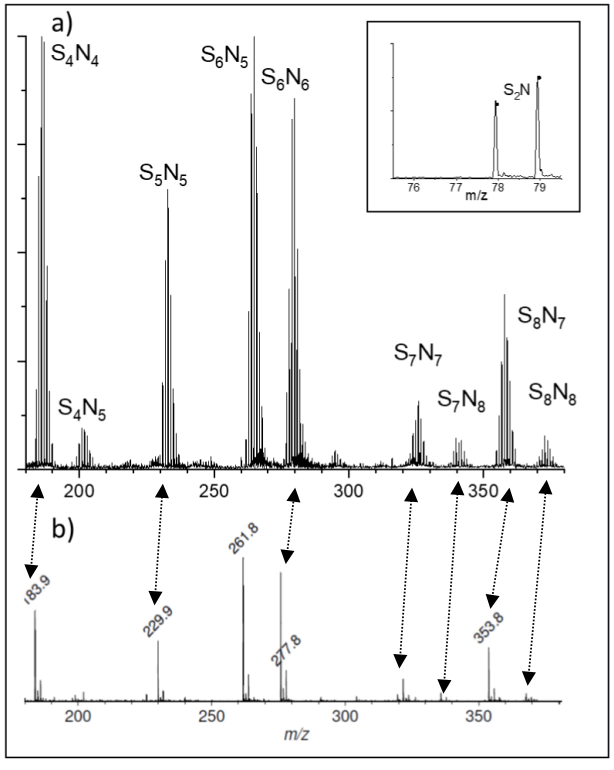

Figure 5. LDI-ToF spectra of (a) $S^{15}N_x$ and (b) $S^{14}N_x$.

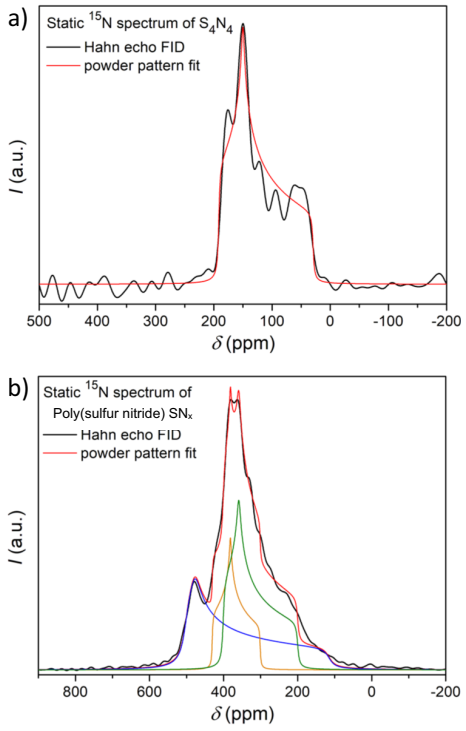

Figure 6. Static ^{15}N spectrum of a) S_4N_4. The red line represents the best powder pattern fit (b) of the poly(sulfur nitride) $S^{15}N_x$. The red line represents the powder pattern fit with three components.

We assume at least three crystallographically different components contributing to the signal. The isotropic chemical shifts of these three components are $R_{iso,1}$ = 320.7 ppm, $R_{iso,2}$ = 371.9 ppm, and $R_{iso,3}$ = 365.6 ppm, respectively. The corresponding asymmetry parameters are η_1 = 0.35, η_2 = 0.7, and η_3 = 0.1, respectively. Due to the low signal-to-noise ratio, it cannot be ruled out that the spectrum consists of more

than three components. In an ideal single crystal with $P2_1/n$ symmetry, all nitrogen atoms would have the identical environment, but it is observed [11] that quite often packing errors occur, e.g., in addition to antiparallel chain orientation of neighboring SN_x chains, although parallel packing is observed. This induces a different environment, leading to the different chemical shifts.

4 Outlook

As already mentioned, superconductivity in SN_x occurs below $T_c = 0.3$ K. Nevertheless, SN_x can be employed for grain boundary engineering together with other superconductors as MgB_2 [14] and YBCO [13]. Fig. 7a shows SN_x fibers grown between MgB_2 grains. Thus, it provides the general possibility of grain boundary engineering [25]. The white arrow indicates the area that was used for EDX analysis (Fig. 7b). The signals belonging to Mg and B from the bulk superconductor and S and N from the SN_x fibers can be identified.

SN_x was also synthesized on a YBCO substrate. Fig. 8a provides an AFM height image. The left part indicates SN_x fibers grown on YBCO whereas the right part provides some details on the YBCO particles. The PF-TUNA image in Fig. 8b maps the electrical conductivity in the picoampere range [26]. Obviously, the SN_x fibers have a higher electrical conductivity at room temperature compared to YBCO. But some parts of the YBCO grains, indicated by the white arrow, show also a higher electrical conductivity than neat YBCO. Some coating of YBCO with SN_x not necessarily as fibers but as thin layers might be responsible for this effect.

In summary, some questions of polymer characterization, such as the molar mass and end groups of SN_x, remain open. Further studies will focus on the electrical and magnetic properties of composite superconductors.

Acknowledgments

We thank Eik Koslowski (Faculty of Natural Science II, Chemistry, Physics, and Mathematics, Martin Luther Univer-

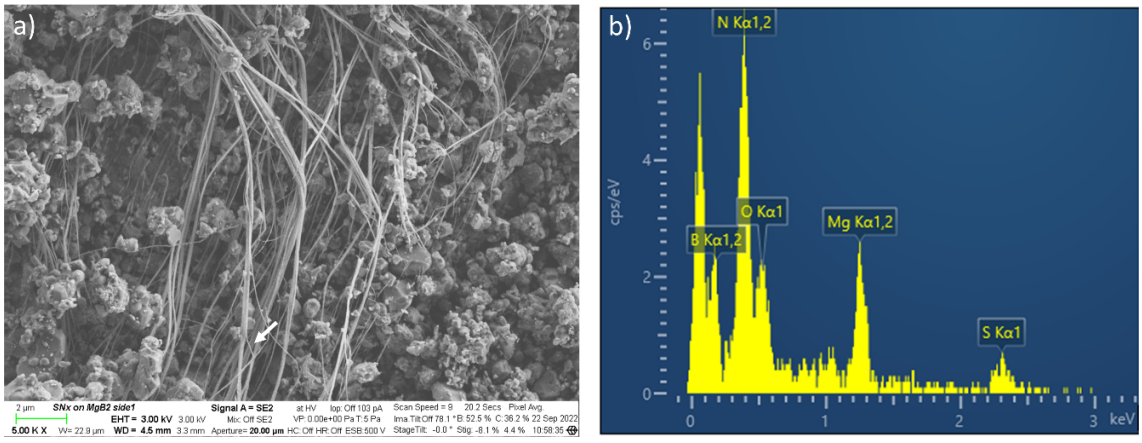

Figure 7. a) SEM image of SN_x polymerized on MgB_2, b) the respective EDX spectrum taken in the area of the white arrow shown in (a).

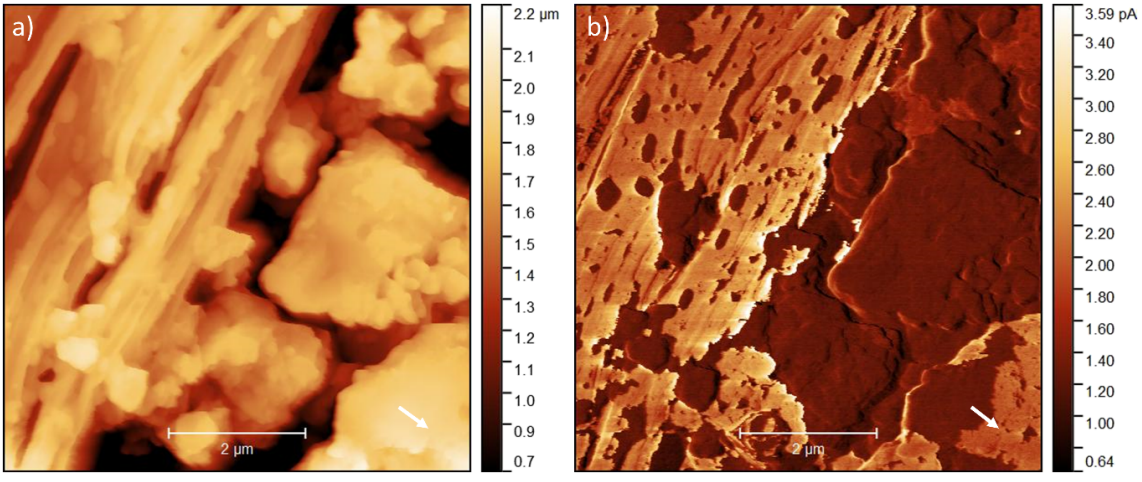

Figure 8. a) SN_x polymerized on YBCO, b) the respective PF-TUNA image.

sity Halle-Wittenberg, Germany) for Raman measurements. Ms. Börner supported all chemical syntheses. Open access funding enabled and organized by Projekt DEAL.

The authors declared no conflict of interest.

Abbreviations

AFM	atomic force microscopy
CSA	chemical shift anisotropy
DC	direct current
EDX	energy dispersive X-ray
FTIR	Fourier transform infrared
IR	infrared
LDI-ToF	laser deposition ionization time-of-flight
MAS	magic-angle spinning
NMR	nuclear magnetic resonance
PF-TUNA	PeakForce tunneling atomic force microscopy
POM	polarized optical microscopy
SEM	scanning electron microscopy
YBCO	yttrium barium copper oxide

References

[1] C. H. Hsu, M. M. Labes, *J. Chem. Phys.* **1974**, *61*, 4640–4645.
[2] R. L. Green, G. H. Street, *Phys. Rev. Lett.* **1975**, *34*, 577–579.
[3] T. T. Takaluoma, K. Laasonen, R. Laitinen, *Inorg. Chem.* **2013**, *52*, 4648–4657.
[4] W. H. Jones, R. D. Bardo, *J. Phys. Chem.* **1993**, *97*, 4974–4983.
[5] N. K, C. S. Rout, *RSC Adv.* **2021**, *11*, 5659–5697.
[6] M. Goehring, D. Voigt, *Z. Anorg. Allg. Chem.* **1956**, *285*, 181–190.
[7] M. M. Labes, P. Love, L. F. Nichols, *Chem. Rev.* **1979**, *79*, 1–15.
[8] A. J. Banister, I. B. Gorrell, *Adv. Mater.* **1998**, *10*, 1415–1429.
[9] T. Chivers, R. S. Laitinen, *Dalton Trans.* **2020**, *49*, 6532–6547.
[10] M. C. Cohen, A. F. Garito, A. J. Heeger, A. G. MacDiarmid, C. M. Mikulski, M. S. Saran, J. Kleppinger, *J. Am. Chem. Soc.* **1976**, *98*, 3844–3848.
[11] G. Heger, S. Klein, L. Pintschovius, H. Kahlert, *J. Solid State Chem.* **1978**, *23*, 341–347.
[12] R. H. Hoel, D. J. Dingley, *J. Mater. Sci.* **1982**, *17*, 2997–3008.
[13] J. G. Bednorz, K. A. Müller, *Z. Phys. B: Condens. Matter* **1986**, *64*, 189–193.
[14] J. Nagamatsu, N. Nakagawa, T. Muranaka, Y. Zenitani, J. Akimitsu, *Nature* **2001**, *410*, 63–64.
[15] W. L. Jolly, M. Becke-Goehring, *Inorg. Chem.* **1961**, *1*, 76–78.
[16] D. Nečas, P. Klapetek, *Cent. Eur. J. Phys.* **2012**, *10*, 181–188.
[17] A. Seeboth, D. Lötzsch, R. Ruhmann, O. Muehling, *Chem. Rev.* **2014**, *114*, 3037–3068.
[18] T. Chivers, R. T. Oakley, O. J. Scherer, G. Wolmershäuser, *Inorg. Chem.* **1981**, *20*, 914–917.
[19] W. Scherer, M. Spiegler, B. Pedersen, M. Tafipolsky, W. Hieringer, B. Reinhard, A. J. Downs, G. S. McGrady, *Chem. Commun.* **2000**, *7*, 635–636.
[20] R. Steudel, *Z. Naturforsch.* **1981**, *36*, 850–858.
[21] E.-C. Koch, M. Sueska, *Z. Anorg. Allg. Chem.* **2021**, *647*, 192–199.
[22] J. W. Macklin, G. B. Street, W. D. Gill, *J. Chem. Phys.* **1979**, *70*, 2425–2430.
[23] S. H. Irsen, P. Jacobs, R. Dronskowski, *Z. Anorg. Allg. Chem.* **2001**, *627*, 321–325.
[24] D. Massiot, F. Fayon, M. Capron, I. King, S. Le Calve, B. Alonso, J.-O. Durand, B. Bujoli, Z. Gan, G. Hoatson, *Magn. Reson. Chem.* **2002**, *40*, 70–76.
[25] H. Hilgenkamp, J. Mannhart, *Rev. Mod. Phys.* **2002**, *74*, 485–549.
[26] E. Amado, N. Hasan, K. Busse, J. Kressler, *Macromol. Chem. Phys.* **2021**, *222*, 2100113.

Research Article: $S_4{}^{15}N_4$ was used for the synthesis of poly(sulfur nitride). The isotope ratio in the labeled polymer was obtained by laser deposition ionization time-of-flight mass spectroscopy. Solid-state ^{15}N nuclear magnetic resonance spectroscopy of $S^{15}N_x$ indicates that at least three different chemical environments for ^{15}N atoms are present in the crystals.

Synthesis and Characterization of ^{15}N-Labeled Poly(sulfur nitride) in Bulk and in Superconductor Composites

Jörg Kressler*, Julian Radicke, Karsten Busse, Konstantin Amsharov, Yury Golitsyn, Detlef Reichert, Frank Syrowatka, Nazmul Hasan

Chem. Eng. Technol. **2023**, *46 (XX)*, XXX … XXX

DOI: 10.1002/ceat.202300141